The Astrophysical Journal, 725:1317–1326, 2010 December 10 doi:10.1088/0004-637X/725/1/1317

ANTI-CORRELATED SOFT LAGS IN THE INTERMEDIATE STATE OF BLACK HOLE SOURCE GX 339−4

K. Sriram[1], A. R. Rao[2], and C. S. Choi[1]
[1] Korea Astronomy and Space Science Institute, Deajeon 305-348, Republic of Korea; astrosriram@yahoo.co.in
[2] Tata Institute of Fundamental Research, Mumbai 400005, India
Received 2010 March 25; accepted 2010 October 10; published 2010 November 24

ABSTRACT

We report the few hundred second anti-correlated soft lags between soft and hard energy bands in the source GX 339−4 using *RXTE* observations. In one observation, anti-correlated soft lags were observed using the ISGRI/*INTEGRAL* hard energy band and the PCA/*RXTE* soft energy band light curves. The lags were observed when the source was in hard and soft intermediate states, i.e., in a steep power-law state. We found that the temporal and spectral properties were changed during the lag timescale. The anti-correlated soft lags are associated with spectral variability during which the geometry of the accretion disk is changed. The observed temporal and spectral variations are explained using the framework of truncated disk geometry. We found that during the lag timescale, the centroid frequency of quasi-periodic oscillation is decreased, the soft flux is decreased along with an increase in the hard flux, and the power-law index steepens together with a decrease in the disk normalization parameter. We argue that these changes could be explained if we assume that the hot corona condenses and forms a disk in the inner region of the accretion disk. The overall spectral and temporal changes support the truncated geometry of the accretion disk in the steep power-law state or in the intermediate state.

Key words: accretion, accretion disks – binaries: close – stars: individual (GX 339−4) – X-rays: binaries

Online-only material: color figures

1. INTRODUCTION

The huge database of *RXTE* observations of different Galactic black holes (GBHs) shows that the spectral and timing properties of the accretion disk in these objects can be constrained depending on the classification schemes (Esin et al. 1997; Grove et al. 1998; McClintock & Remillard 2004; Belloni 2010; McClintock et al. 2009). During the rise and fall of the outburst the accretion disk is found to be in the low–hard (LH) state where the hard component (power-law index $\Gamma \sim 1.5$) is strong, most probably due to the presence of a Compton cloud or a jet, along with an extremely weak or undetected soft component (presumably due to a Keplerian disk). The power density spectrum (PDS) in this state shows a strong band-limited noise, occasionally with quasi-periodic oscillations (QPOs) at low frequencies. On the other hand, when the soft X-ray intensity increases, the hard component becomes very weak and the soft component dominates the spectrum along with the disappearance of a QPO feature in the PDS. This state is known as the thermal-dominated (TD) state (Kubota et al. 2001; Remillard & McClintock 2006) or the high–soft (HS) state (Belloni 2010). Both classification schemes point toward a similar picture, where the accretion disk approaches close to the black hole, when the source moves from the LH to the TD state.

The evolution of the accretion disk from the LH state to the HS state and vice versa is not only complicated but also poorly understood. It is generally believed that when the mass accretion rate increases from the LH state, the strength of the soft component increases relative to that of the hard component, which softens. Since the spectrum is steep (power-law index $\Gamma \geqslant 2.5$) and, in most of the GBHs, the X-ray luminosity is high, this state is termed the steep power-law (SPL) state or the very high (VH) state (Miyamoto et al. 1991; Remillard & McClintock 2006). The complexity of this state is unveiled by study of the hardness intensity diagram (HID), which is found to be a useful phenomenological tool to trace the evolution of the accretion disk during an outburst (Belloni et al. 1996; Mendez & van der Klis 1997; Belloni 2010). This unified scenario is further constrained by radio observations (Corbel et al. 2000; Gallo et al. 2003; Fender et al. 2004; Fender et al. 2009).

This transitional state is further divided into two states, i.e., a hard intermediate state (HIMS) and a soft intermediate state (SIMS); for further details, see Belloni 2010 and references therein. X-ray and radio studies show that the HIMS–SIMS transition can be approximated as being due to the crossing over of a "jet line" in the HID; however, further observations in this state are needed to constrain this picture as the track of the jet line in the HID is still not clearly understood (Fender et al. 2009). In the temporal domain, the most important property of this state is the presence of high-frequency QPOs $\geqslant$ 100 Hz (HFQPO) together with the intermediate (IM) QPOs in the frequency range of 1–10 Hz (Casella et al. 2004; Remillard & McClintock 2006; Belloni 2010). In the spectral domain, perhaps the most important physical property of the SPL/IM state is the presence of a low temperature ($\leqslant$10 keV), high optical depth (2–5) Compton component, possibly coming from a compact cloud close to the black hole (Done & Kubota 2006; Sriram et al. 2007, 2009; Caballero-García et al. 2009). This is found that as the disk approaches or recedes from the black hole, the QPO frequency increases or decreases (Done et al. 2007). The broadband spectrum shows a hard component which is possibly due to thermal Comptonization of soft photons in the Compton cloud (Done & Kubota 2006; Sriram et al. 2007, 2009). This could be the most favorable mechanism in this state because both the soft and hard components dominate and this spectral characteristic is less prominent in other spectral states. In this state, the temporal and spectral transitions are fast and distinct (these states cover a large fraction of the HID plane) when compared to the other states (Dunn et al. 2010). It is found that in the IM/SPL state the accretion disk is truncated and hence the coupled soft/hard emission regions show

anti-correlated lags which constrain and strengthen the truncated geometry model.

There have been numerous studies on lags that range from a few milliseconds to a few hundred seconds. Small-scale (few milliseconds) positive and negative lags have been found in GRS 1915+105 (Cui 1999; Lin et al. 2000; Reig et al. 2000). Previous researchers have found that the observed lags are frequency dependent. Similar results were obtained for XTE J1550−564 (Cui et al. 2000). More detailed studies were carried out for XTE J1859+226, which shows that B-type QPOs always show a hard lag, whereas the A-type and C-type QPOs show only the soft lag. They argued that the energy dependence of QPOs rules out the possibility of a simple disk origin and that the 6 Hz QPO is related to unknown fundamental processes (Casella et al. 2004). Recently, it was found that, in the case of GRS 1915+105, the lags are both frequency and energy dependent (Qu et al. 2010), which rules out the existing possible models of low-frequency QPO production. These small Fourier lags strongly favor the Comptonization process close to the black hole and the lag time corresponds to the energy gain time in the Compton cloud or probably in the base of the jet.

The few hundred second scale lags were first reported in the source Cyg X-3. The cross-correlation between the soft and hard energy bands shows anti-correlated hard lags along with spectral pivoting (Choudhury & Rao 2004). Later, similar anti-correlated hard lags were found in several black hole sources, GRS 1915+105, XTE J1550−564, and H1743−322 (Choudhury et al. 2005; Sriram et al. 2007, 2009), and in one neutron star source, Cyg X-2 (Lei et al. 2008). It was found that along with spectral pivoting the centroid QPO frequency is shifted during the observed lag timescale. The soft and hard fluxes were anti-correlated during these lags and altogether the results suggest that, as the disk front moves toward the black hole, the soft photons cool the Compton cloud, changing the geometrical or physical size. Until now, soft lags were often observed in smaller dynamical scales but anti-correlated soft lags were not observed on a longer timescale.

Here we report the discovery of anti-correlated soft lags in the black hole source GX 339−4. GX 339−4, a microquasar, has an orbital period of ∼1.7 days, with a mass function $f(M) = 5.8 \pm 0.5\ M_{\odot}$ (Hynes et al. 2003). The secondary companion is an F-type subgiant star situated at a distance of 6–15 kpc (Hynes et al. 2004; Zdziarski et al. 2004). Based on spectroscopic studies, the binary inclination of this system was found to be low, i.e., $i = 15^{\circ}$ (Wu et al. 2001). GX 339−4 may harbor a black hole with a high spin parameter of $a = 0.8$–0.9 (Miller 2007). The radio observations during the state transition suggest discrete ejection events along with relativistic radio jets with speed $v/c > 0.9$ (Gallo et al. 2004). GX 339−4 was the first source to exhibit features of the VH state (Miyamoto & Kitamoto 1991). The source had an outburst during the year 2006–2007 which was continuously monitored by the *RXTE* satellite. The outburst lasted about 10 months during which *RXTE* made 220 pointed observations. The detailed spectral and temporal analysis of 83 observations covering the transition from the LS state to the HS state has been carried out by Motta et al. (2009). They found that the high-energy cutoff initially decreased during the hard IM state and increased in the soft IM state, implying a sudden change in the high-energy radiative mechanism close to the black hole. This outburst was also observed by the the *XMM-Newton* and *International Gamma-Ray Astrophysics Laboratory* (*INTEGRAL*) satellites and the results are presented in Del Santo et al. (2009) and Caballero-García et al. (2009).

We have used HIMS/SIMS classified observations to find the lags between the soft and hard energy bands using *RXTE* observations. In three observations, we found anti-correlated soft lags of the order of a few hundred seconds along with a shift in the centroid frequency of the QPO. We also found that the spectral properties changed during these observations. In one of the observations where anti-correlated soft lag was found, the PCA/*RXTE* soft energy band (2–5 keV) and ISGRI/*INTEGRAL* hard energy band (20–40 keV) also simultaneously showed anti-correlated soft lag. The temporal and spectral variations during the detected lags are explained in the framework of a truncated disk geometry. Re-condensation of hot flow is proposed to understand the shift in the QPO frequency and spectral changes in the respective observations.

2. DATA REDUCTION

The 2006–2007 outburst in GX 339−4 was extensively observed by the *RXTE* satellite (Swank 1999). The satellite is comprised of three onboard detectors, the Proportional Counter Array (PCA; Jahoda et al. 2006), High-Energy X-ray Timing Experiment (HEXTE; Rothschild et al. 1995), and All-Sky Monitor (ASM; Levine et al. 1996). Detailed temporal and spectral studies have been carried out during the outburst and the respective observations were classified into three canonical states (Motta et al. 2009). Motta et al. found that out of 83 observations, 15 belong to the HIMS and 4 belong to the SIMS classification. We have obtained the cross-correlation function (CCF) for the HIMS and SIMS classified light curves. We have used the PCA data, which show the characteristics of the HIMS and SIMS classification scheme. For spectral studies, we have extracted the spectra from the top layer of the PCU2 data, which is the most well calibrated among the PCUs, and 0.5% systematic errors are added to the PCA spectrum. To study the PDS, we used the single-bit data mode. We have used HEASOFT v6.8 software to reduce the data and XSPEC v12.5 (Arnaud 1996) for the spectral fittings.

During this outburst, the *INTEGRAL* satellite observed the source on five different days (for more details, see Caballero-García et al. 2009). *INTEGRAL* (Winkler et al. 2003) carries on board two main gamma-ray instruments, the Spectrometer on *INTEGRAL* (SPI, 20 keV–8 MeV; Vedrenne et al. 2003) and the Imager on-Board *INTEGRAL* Satellite (IBIS, 15 keV–10 MeV; Ubertini et al. 2003; Lebrun et al. 2003), as well as two monitoring instruments in the X-ray and optical range, the Joint European X-Ray Monitor (JEM-X, 3–35 keV; Lund et al. 2003) and the Optical Monitoring Camera (OMC; Mas-Hesse et al. 2003). We have used *INTEGRAL*/ISGRI data (SCW ObsID: 053600360010) for further reduction and analysis. We have used the IBIS_SCIENCE_ANALYSIS main script to obtain the light curve in the 20–40 keV energy band. Data reduction was carried out using the Off-line Science Analysis (OSA) v8.0 package. To obtain the lag time we closely follow the method described in Sriram et al. (2007). An inverted Gaussian function is used to fit the cross-correlation spectra and the error bars shown are at the 90% confidence level throughout this paper.

3. ANALYSIS

3.1. Temporal Analysis

The background-subtracted light curves were obtained in two energy bands, the soft (2–5 keV) and hard (20–50 keV) energy bands. We have used the *crosscor* program to look for the anti-correlated lags and discovered anti-correlated soft lags of a

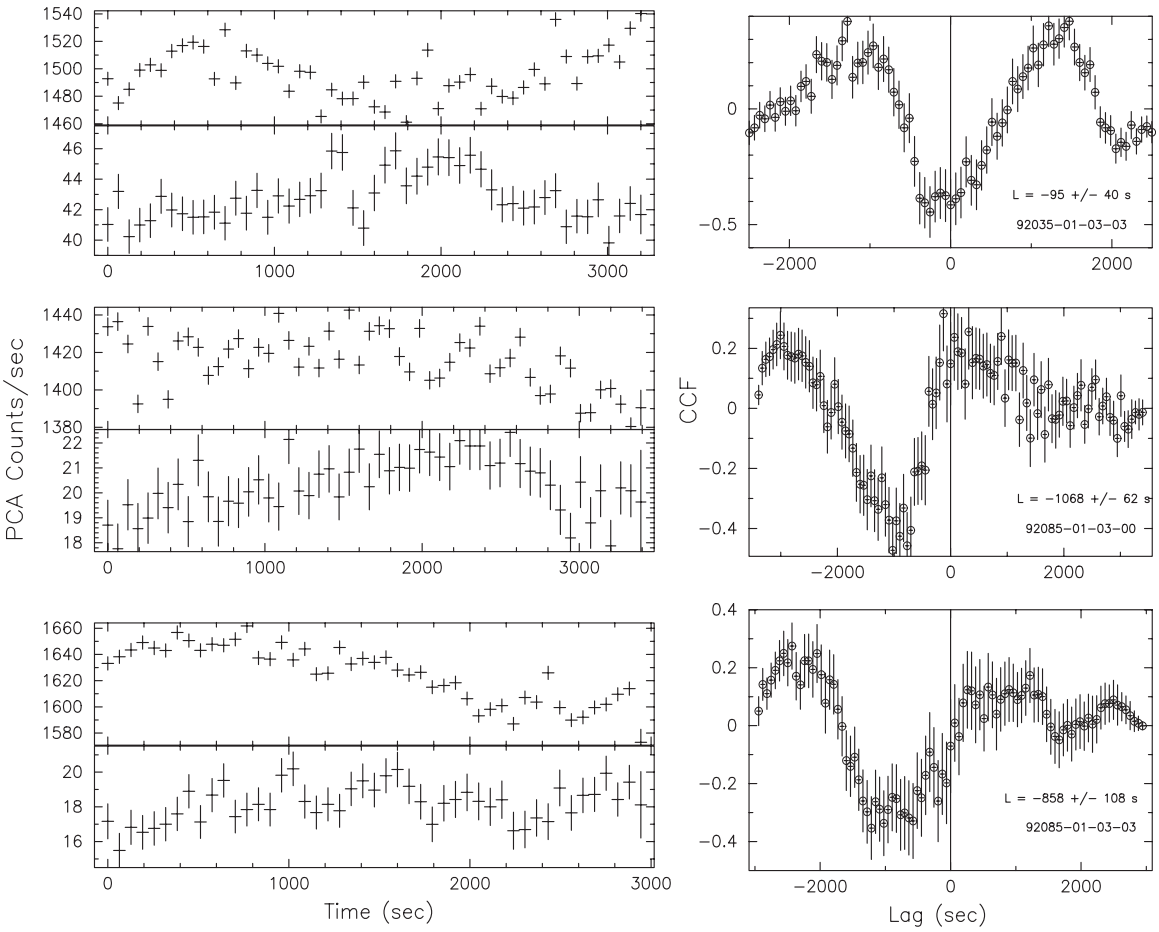

Figure 1. Left: the PCA soft (2–5 keV, top) and hard (20–50 keV, bottom) X-ray light curves of GX 339−4 are shown for three observations. Right: CCFs are plotted for the respective observations and the vertical line represents zero lag. The measured lags (L) and observation ID for each observation are also shown.

few hundred seconds in the three observations (Figure 1). In one case, the cross-correlation is performed between the PCA/*RXTE* soft energy band and the nearly simultaneous ISGRI/*INTEGRAL* hard energy band (20–40 keV). The CCF is found to be asymmetric and an anti-correlated soft lag is observed (Figure 2).

For the three observations shown in Figure 1, the derived values of anti-correlation (minimum values of CCF) are -0.44 ± 0.11, -0.47 ± 0.12, and -0.35 ± 0.10, respectively. The probabilities of getting more than these values, due to random fluctuations in the data, are 1.09×10^{-4}, 3.73×10^{-5}, and 1.60×10^{-3}, respectively (Bevington & Robinson 1992). The derived values of the lags are -95 ± 40 s, -1068 ± 62 s, and -858 ± 108 s, respectively. Treating the estimated error as 1σ (it should be noted that we have used the criterion of $\Delta\chi^2 = 4.0$, typically signifying a 90% confidence level), the lags are detected at confidence levels of 2.4σ, 17.2σ, and 7.8σ, respectively, for the three observations. The corresponding value for the *INTEGRAL*/PCA anti-correlation has a CCF value of -0.49 ± 0.21 (significant at a level of 5.90×10^{-2}), with a lag detected at -352 ± 102 s (a 3.5 σ detection). Hence, we can conclude that the lags are detected at a very high significance level.

It is quite possible that black hole sources like GX 339−4 have long time variabilities, and sampling these light curves at shorter timescales (a few thousand seconds of observations) might cause spurious peaks in the CCF when a "high" point in one light curve hits a "high" or "low" point in another light curve. But the fact that the anti-correlations are observed in the *RXTE* as well as the *INTEGRAL* data shows that the observed anti-correlations are not due to any instrumental artifacts. Further, the low- and high-energy light curves pertain to the same source and hence they are unlikely to show totally independent variations. In order to rule out such spurious possibilities, we have generated two independent simulated light curves of long duration (2^{20} s), using the method of Timmer & Koenig (1995). The simulated light curves were produced using the mean (1415 counts s^{-1}), standard deviation (15 counts s^{-1}), and PSD power-law index ($\beta = -1.30$) of the soft energy band light curve of the second observation (Figure 1). The two light curves are resampled as the original data (bin size of 64 s). A randomly varying number with mean of 1.0 (standard deviation 0.20) was generated using the "randomn" function available in Interactive Data Language (IDL). We smoothed this series using the "SMOOTH" function (available in IDL). The "SMOOTH" function filters an input series using a running-mean top with a given kernel size. We have used kernel size 3 to smooth the series. After doing this the standard deviation was found to be 0.12. Then, one of the light curves is multiplied with the obtained smoothly varying number (variation is random in nature) with a mean of 1.0, which is uncorrelated to the real variability. We have taken 3000 s segments from the simulated light curves and perform cross-correlation analysis. We found that most of the CCFs show anti-correlation and positive-correlation coefficients $\sim \pm 0.25$ and a few segments of the CCFs show low anti ($\leqslant -0.4$) and high positive ($\geqslant 0.4$) cross-correlation coefficients (Figure 3). The observed (Figure 1) anti-correlation coefficient

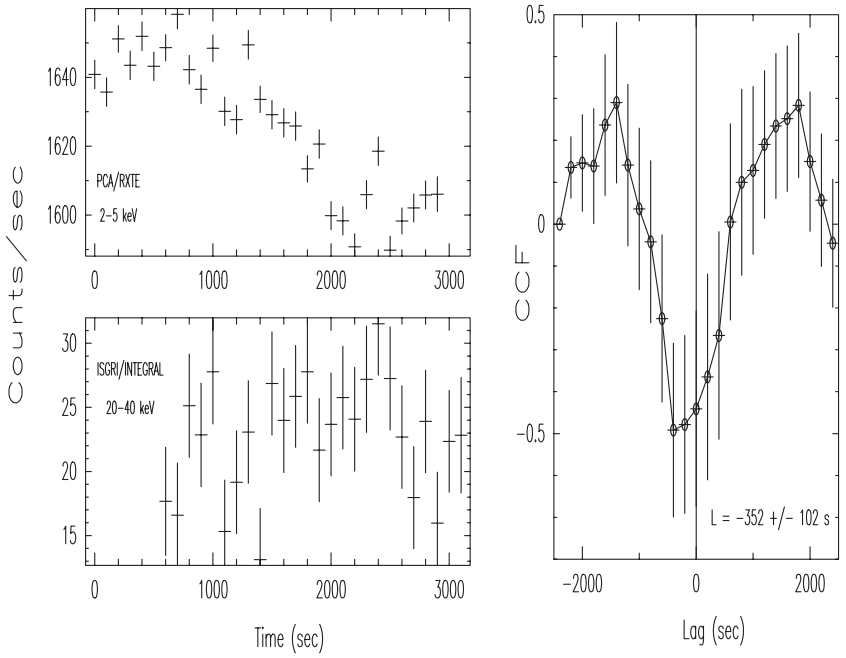

Figure 2. Left: the PCA/*RXTE* soft (2–5 keV, top, ObsID: 92085-01-03-03) and ISGRI/*INTEGRAL* hard (20–40 keV, bottom, SCW ObsID: 053600360010) X-ray light curves are shown. Right: the CCF is plotted. The vertical line represents zero lag and L is the lag timescale.

for the first and second observations is around $\leqslant -0.4$ and the simulation result shows that only 6 segments (out of 350 segments; only 1.8%) show anti-correlation coefficients less than ~ -0.4. This indicates that the observed anti-correlation is significant at >98% confidence level. Apart from the "SMOOTH" function, we have used the "MEDIAN" function and the SAVGOL (Savitzky–Golay) filter (both available in IDL) to smooth the varying number of mean 1. The SAVGOL filter uses a weighted moving average technique. Using both the techniques, we carried out the simulation and found that 8–10 segments (out of 350 segments; 2.2% and 2.8%) show an anti-correlation coefficient less than ~ -0.4.

GX 339−4 is the first black hole source to show anti-correlated soft lags at such large timescales. The soft lag means that the soft photons are lagging compared to the hard photons.

The observation time (MJD 54163) of the third observation (ObsID: 92085-01-03-03) matches the peak of a small magnitude hard re-flare as depicted from both HEXTE and *Swift*/BAT light curves (Motta et al. 2009; Caballero-García et al. 2009). In this episode, the sudden increase in the hard flux might be due to the ejection of the inner hot disk or corona (which is often observed in GX 339−4 during this state; Gallo et al. 2004) but the radio observations during this episode were lacking and hence an exact production mechanism for the second hard re-flare is difficult to understand.

GX 339−4 showed A, B, and C types of QPOs during the 2006–2007 outburst (Motta et al. 2009). In three observations where soft lags are observed, C-type QPOs are present (Motta et al. 2009). In order to investigate the small dynamical changes during the observations where lags are detected, we have extracted the PDS in the initial (part A) and final (part B) parts of the light curves. These fitted PDSs are plotted in Figure 4. The PDSs are fitted with a broken power-law + Lorentzian model. We found that the centroid QPO frequencies are shifted to lower frequencies, implying that the physical regions responsible for the QPOs have changed during the respective observations (see Figure 4 and Table 1). Generally,

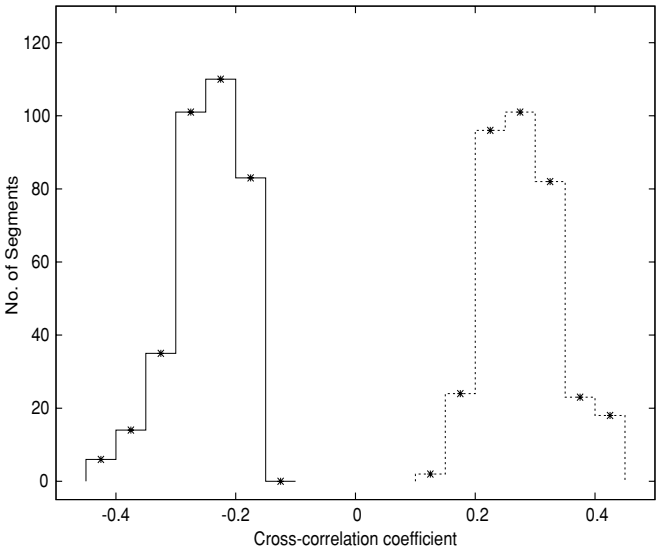

Figure 3. Histogram showing the anti-correlation (thick line) and positive-correlation (dashed line) coefficients vs. the number of segments, each with a length of 3000 s. The number of segments with an anti-correlation coefficient $\leqslant -0.4$ occupies a minute fraction of area in the histogram and is only 1.8% of the total segments, indicating that the observed anti-correlation is not spurious.

it is observed that, as the QPO frequency increases, the width of the QPO also increases, changing from a type-C QPO to a type B and then to a type A one (Casella et al. 2005). The QPO profile is often fitted with a Lorentzian but as its shape changes from a type C to type A, a Gaussian function is preferred (Belloni 2010). In the second and third observations, the shift in the QPO centroid frequency is relatively larger ($\delta f_c \sim 1$ Hz) compared to the first observation ($\delta f_c \sim 0.2$ Hz; Figure 4). The production mechanism of low-frequency QPOs (LFQPOs) and the respective locations on the accretion disk are still a matter of debate but often these QPOs are attributed to

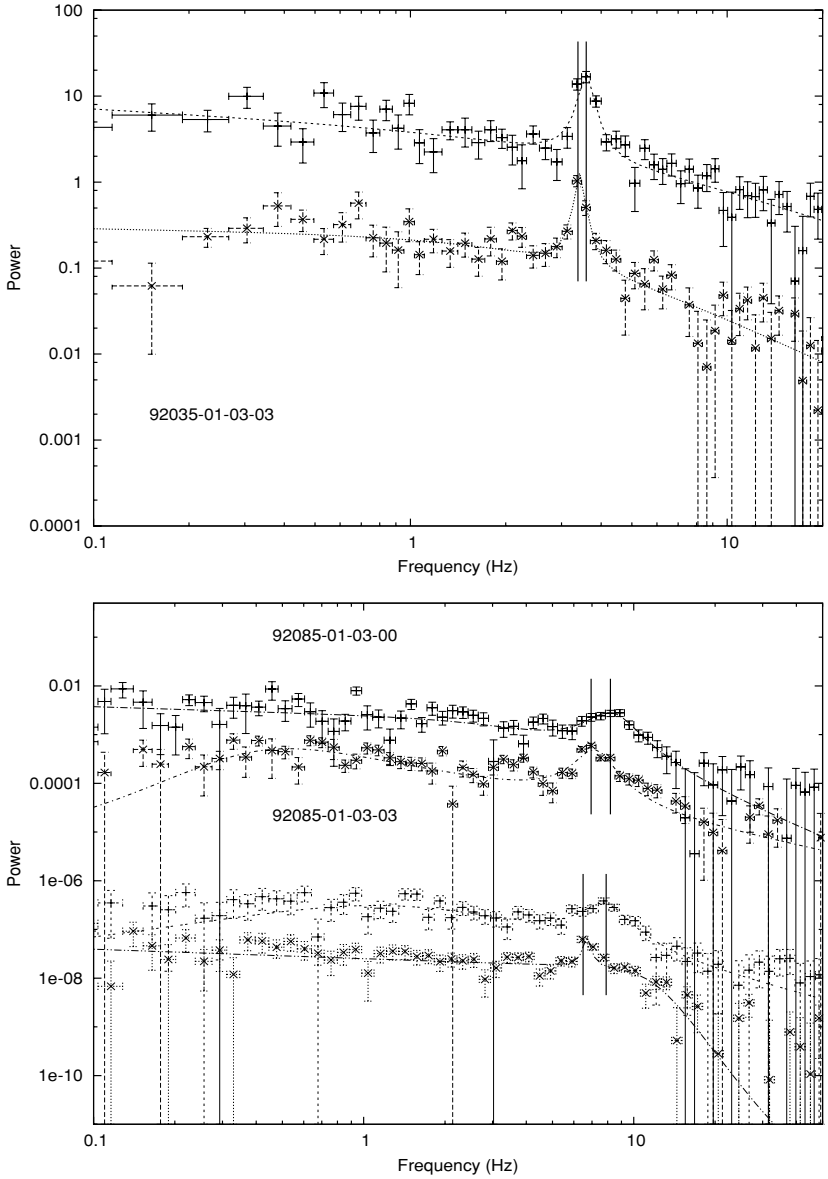

Figure 4. PDS for the three observations (top panel: 92035-01-03-03; bottom panel: 92085-01-03-00, 92085-01-03-03). For each observation, the upper PDS corresponds to the part A section and the lower PDS corresponds to the part B section of the light curves. The vertical line highlights the shift in the observed centroid frequency. The power is the normalized power in units of $(\mathrm{rms/mean})^2\ \mathrm{Hz}^{-1}$. In the bottom panel, the PDSs are appropriately shifted on the vertical scale for clarity.

the Comptonization region in the accretion disk, which is generally assumed to be located at the inner region of the disk (Chakrabarti & Manickam 2000; Titarchuk & Fiorito 2004). Sometimes, LFQPOs are related to the propagation of a truncated disk front through the hot flow in the accretion disk (Done et al. 2007).

During our analysis, we found that in two observations, ObsId: 92085-01-01-05 and 92085-01-02-05, the QPO features are present in the respective PDSs but are not mentioned in the work of Motta et al. (2009). These observations were classified as the HS state as per the Belloni (B) classification and the IM state as per the McClintock and Remillard (MR) classification scheme (see Table 1 in Motta et al. 2009). It is found that in ObsID: 92085-01-02-05, the QPO feature is not present in the 2.06–5.71 keV energy band but is seen only in the 6.12–14.76 keV band (single-bit mode data are used), whereas in ObsID: 92085-01-01-05, the QPO feature is present in both energy bands (generic binned mode data; Figure 5). The power-law + Lorentzian model is used to fit the PDS in ObsID: 92085-01-01-05 and the broken power-law + Lorentzian model is used in the other observation. In Figure 5, the respective PDSs are fitted with and without the QPO feature. The dashed line shows the fit with the QPO feature and the solid line shows the fit without it. The residuals are plotted with respect to the simple power-law and broken power-law models for each observation (Figure 5). We find a $\delta\chi^2$ value of 82 ($\chi^2 = 198.10$ without QPO, $\chi^2 = 116.10$ with QPO for dof 71) and $\delta\chi^2 = 71.32$ ($\chi^2 = 144.40$ without QPO, $\chi^2 = 73.08$ with QPO for dof 63), respectively, for the two observations. The high $\delta\chi^2$ values clearly indicate the presence of a QPO feature. The centroid frequency of QPO in ObsID: 92085-01-01-05 is found to be at $f_c = 4.91 \pm 0.12$ Hz with a quality factor $Q = f_c/\delta f = 3.14$, whereas in the other observation, the centroid frequency is found to be at $f_c = 10.70 \pm 0.24$ Hz with a quality factor $Q = f_c/\delta f = 2.20$. Since the QPOs in the respective observations are strong properties of the IM state, we conclude that these

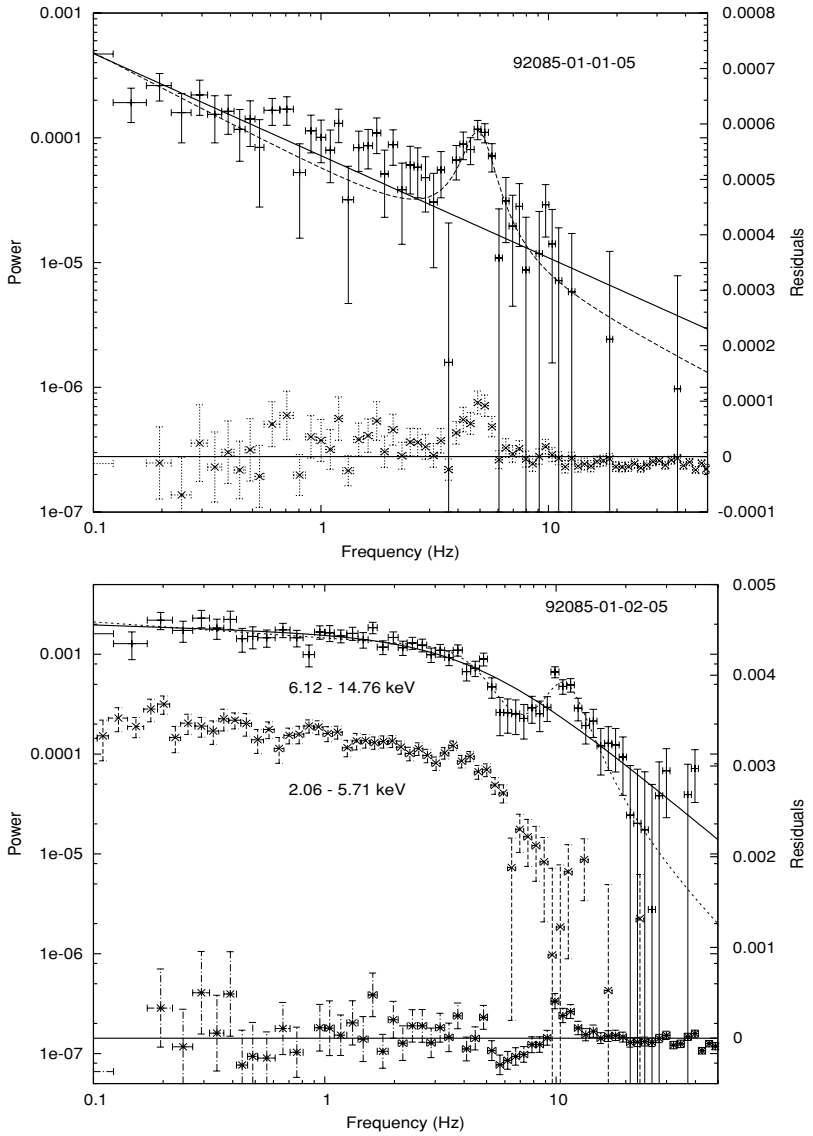

Figure 5. Fitted PDS for two observations (top: 92085-01-01-05; bottom: 92085-01-02-05). For both observations, the PDS is fitted with and without the QPO feature. In each panel, the dashed line shows the fit with the QPO and the solid line shows the fit without the QPO. In the bottom panel, both the energy band PDSs (2.014–5.71 keV PDS is shifted by a factor of 0.5 for clarity) are shown and the QPO feature is clearly seen in the higher energy band. At the bottom of each panel, the residuals are clearly visible around the QPO feature. The power is in units of $(\mathrm{rms/mean})^2\ \mathrm{Hz}^{-1}$.

two observations belong to the IM state rather than the HS state.

3.2. Spectral Analysis

The temporal analysis shows large-scale lags and a prominent shift in the centroid frequencies in the second and third observations compared to the first. Hence, we perform a detailed spectral analysis for the last two observations. The model-independent spectral ratios (the ratio of the part A spectrum to the part B spectrum) are shown in Figure 6 and they show a pivoting feature in the low energy range (4–5 keV) which indicates that the probable changes are occurring at lower energies. We have fitted the 2.8–30.0 keV spectra of the initial and final parts (the same parts used to obtain the PDS) of the respective observations and unfolded a model consisting of a disk blackbody, power law, and absorption, along with a Gaussian line (model: wabs*(diskbb+Gaussian+power-law in XSPEC). The equivalent hydrogen column density is fixed at 0.5×10^{22} cm^{-2} (Dickey & Lockman 1990), the Gaussian line energy is fixed at 6.4 keV, and the remaining parameters were set free during the fitting procedure. The unfolded spectra for parts A and B are shown for the third observation (ObsID: 92085-01-03-03) in Figure 7. It is clear from the figure that the pivoting is caused by changes in the disk normalization and power-law index components which explain the model-independent pivoting. We found that all other parameters except for the disk temperature varied significantly between parts A and B in the individual observations (Table 1). The unabsorbed soft and hard fluxes were anti-correlated between the initial and final parts and it was found that the disk flux decreases with a simultaneous increase in the power-law flux (Table 1). These differences indicate that during the observed lag timescale the spectrum has comprehensively changed. In order to show the prominent differences in the spectra between parts A and B, we have used the part A spectrum model parameters to fit the part B spectrum and plotted the $\delta\chi$ (i.e., residuals in terms of sigmas with error bars) for both parts in Figure 8. It can be seen that there is an excess in the 6–15 keV energy region, which indicates

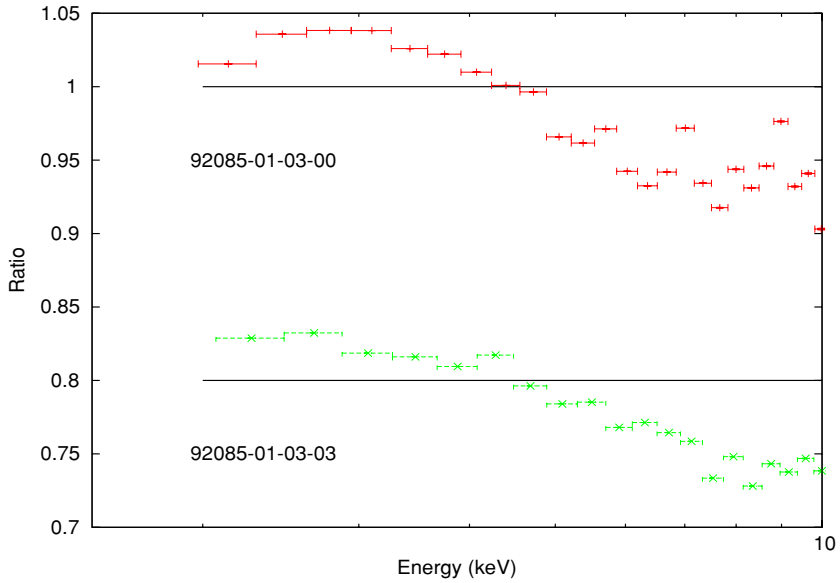

Figure 6. Spectral ratios of the initial and final parts (A and B) of the second and third observations are shown. The data for the third observation are shifted vertically downward for clarity. For both observations, the pivot point is found to be around 4–5 keV.
(A color version of this figure is available in the online journal.)

Table 1
Details of the Spectral and Temporal Parameters in Individual Parts of the Respective Observations

Parameters	92085-01-03-00		92085-01-03-03	
	A	B	A	B
$kT_{\rm in}$[a]	0.87 ± 0.007	0.84 ± 0.008	0.86 ± 0.006	0.85 ± 0.01
$N_{\rm bb}$	2014 ± 100	1827 ± 111	1955 ± 77	1758 ± 83
$\Gamma_{\rm Pl}$[b]	2.42 ± 0.05	2.59 ± 0.04	2.40 ± 0.04	2.51 ± 0.04
$N_{\rm Pl}$[c]	4.06 ± 0.72	6.46 ± 0.80	3.56 ± 0.42	5.08 ± 1.02
χ^2/dof	54/55	40/55	49/46	64/49
Disk flux[d]	9.15	7.34	8.78	7.44
Power-law flux	8.47	10.18	7.95	9.26
Delay (s)	−1068 ± 62	...	−858 ± 108	...
f (Hz)[e]	8.15 ± 0.33	7.04 ± 0.15	7.64 ± 0.35	6.67 ± 0.18

Notes. A and B correspond to the initial and final parts of the observation, respectively.
[a] Disk temperature using a diskbb model.
[b] Power-law index.
[c] Power-law normalization.
[d] The flux unit for all the models is 10^{-9} erg cm^{-2} s^{-1}.
[e] QPO centroid frequency and PDSs are fitted with a power-law + Lorentzian model.

that during the lag timescale there is an increase in flux in the said energy domain.

4. DISCUSSION AND CONCLUSION

The spectral and temporal properties of accretion disks in black holes can be explained using the framework of a truncated disk geometry. In the LH state, the disk is assumed to be truncated at a large radial distance and as the disk approaches the last stable orbit, it becomes non-truncated, resembling the properties of the TD state. Recent *RXTE*, *XMM-Newton*, and *Chandra* observations found a cool thermal component in the LH state (Reis et al. 2009, and references therein) but more observational studies are required to establish the geometrical picture in this state. Our detailed spectral and temporal results from the study of various black hole sources, GRS 1915+105, XTE J1550−564, and H1743−322, show that in the IM state/SPL state, the accretion disk is truncated very close to the black hole and the truncation radius (r_t) is around $\sim r_t \leqslant 25 r_s$ (where r_s is the Schwarzschild radius; Choudhury & Rao 2004; Choudhury et al. 2005; Sriram et al. 2007, 2009). Similar anti-correlated hard as well as soft lags were found in one neutron star source (Cyg X-2) during which the spectrum changes at different pivoting energies (Lei et al. 2008). These results are very important as they show that the accretion disk is truncated, i.e., a radially moving Keplerian disk along with a Compton cloud/base of jet most probably located close to the black hole.

In this paper, we report the discovery of anti-correlated soft lags of the order of a few hundred to thousand seconds (Figure 1). The anti-correlated soft lag is further supported by the ISGRI/*INTEGRAL* hard energy band in the third observation (ObsID: 92085-01-03-03, Figure 2). The CCF between the PCA/*RXTE* (2–5 keV) and ISGRI/*INTEGRAL* (20–40 keV) was found to be anti-correlated with a negative lag timescale. This lag timescale is a few hundred seconds smaller than the lag obtained using the PCA/*RXTE* data. This may be due to the fact that the simultaneous observation times from *RXTE* and *INTEGRAL* are of shorter duration. During the observed lags, the physical properties of the inner region are changed; this fact is further supported by the study of the PDS of the respective observations. It was found that the QPO centroid frequencies have been shifted to a lower frequency in a single observation. There is no clear consensus as to which physical component (Compton cloud or disk) is responsible for the production of LFQPOs. Recently, Cabanac et al. (2010) showed that an oscillating hot corona is able to produce the LFQPOs well, assuming a truncated disk geometry. According to this model, a phase lag of π between the low and high energy bands is seen (see their Figure 8), which is a strong prediction of the truncated geometry. These theoretically predicted variabilities closely match the first observation light curves where a ∼100 s anti-correlated soft lag was observed (Figure 1). In the Cabanac et al. (2010) model, the

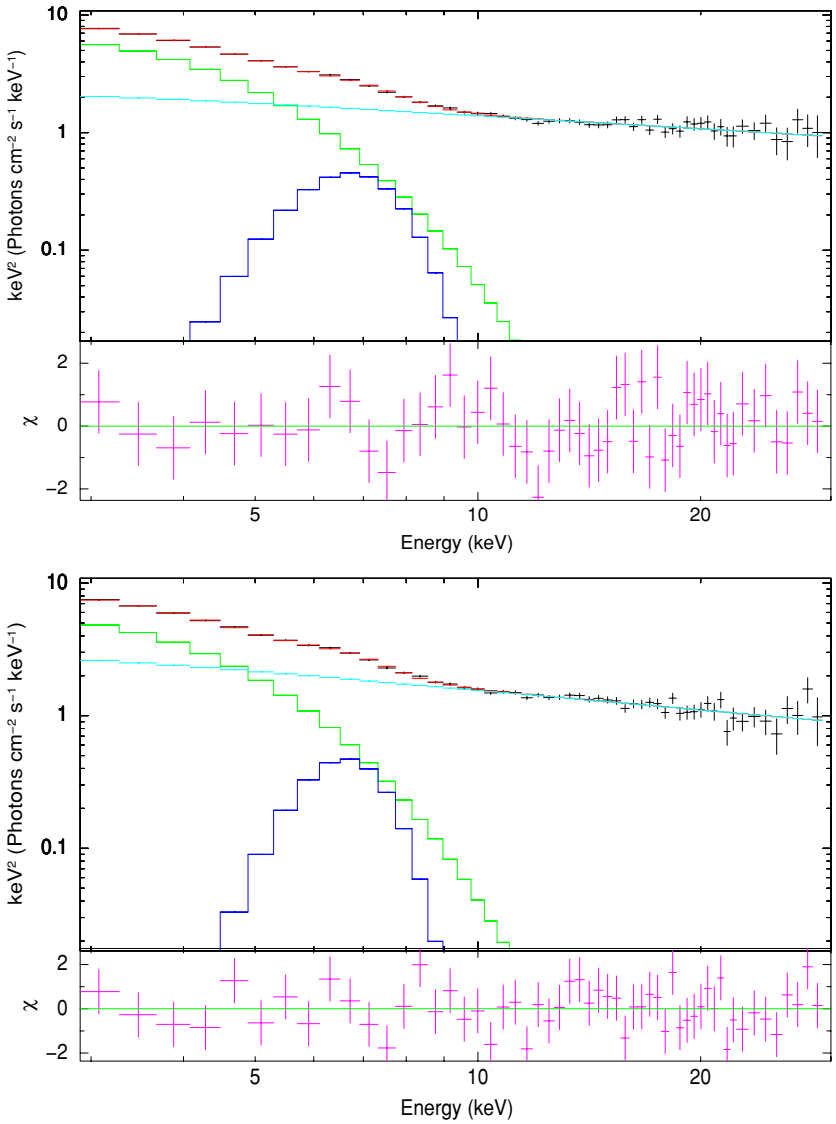

Figure 7. Unfolded spectra along with $\delta\chi$ are shown for parts A and B for the observation ObsID: 92085-01-03-03. The model-dependent pivoting point agrees with the model-independent pivoting point in the respective spectra around ∼5 keV.

(A color version of this figure is available in the online journal.)

QPO propagates toward higher frequency as the radius of the corona front moves toward the black hole, whereas we find that a shift in the disk inner radius is decreased ($\propto$ disk normalization) for a few percentile change in the QPO frequency. This is due to the fact that the boundary (inner front) where the disk truncates and the Compton cloud dominates could be the same, and hence, similar results were observed. The shift in the centroid frequency to lower values (Figure 4) indicates that the corona front/disk front is moving away from the black hole, resulting in an increase in the hard X-ray flux which is clearly seen in the $\delta\chi$ plot (Figure 8).

In the spectral domain, it is clear that, except for the disk temperature, all other parameters were significantly varied in a single observation between parts A and B (Table 1). The most important parameters are the soft and hard fluxes which change in an opposite manner, i.e., the soft flux decreases with an increase in the hard flux (Table 1). The power-law index steepens with an increase in the power-law normalization. The observed anti-correlated soft lags are associated with the spectral variability during which the geometry of the accretion disk changes. The gravitational heating and Compton cooling are continuous processes in the accretion disk and the truncation of the disk is most probably due to changes in the level of Compton cooling mechanism, which is further related to the disk soft photon flux ($\propto$ mass accretion rate). As the disk size increases, the number of soft photons increases, which cools down the Compton cloud and vice versa. Our spectral results show that the disk normalization decreased, implying that the disk inner front is moving toward the black hole which cools the Compton cloud (the power-law index steepens). The PDS study shows that the QPO centroid frequency shifted to a lower frequency which indicates an increase in the disk/corona inner front. These observed contradictory features can be explained if we assume that the inner hot flow (ADAF) condenses back onto the inner disk, relatively increasing the size of the disk, steepens the power-law index, and increases the hard flux. The IM state is the most probable phase of accretion where the condensation of the inner hot matter can transform into an inner disk (Meyer-Hofmeister 2004; Meyer et al. 2007; Liu et al. 2007). More studies are required to understand this phenomenon (if it

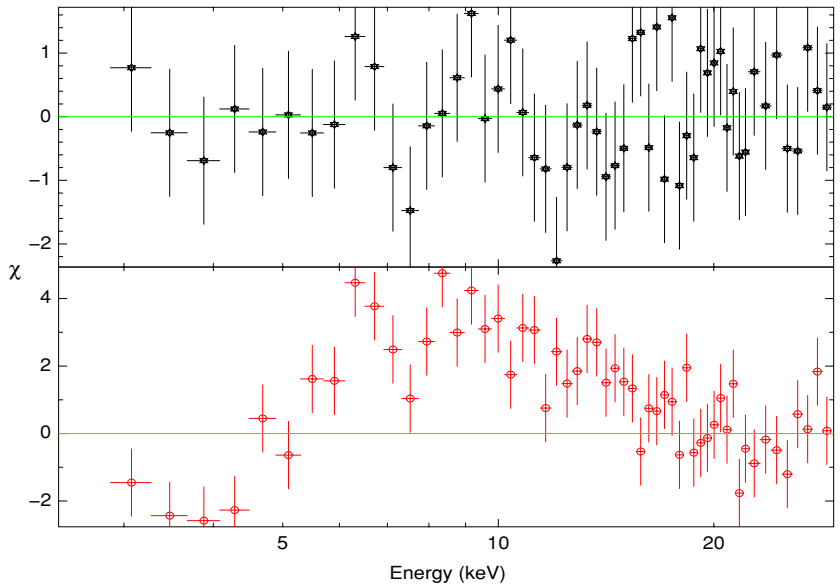

Figure 8. $\delta\chi$ for part A (top) and part B (bottom) for ObsID: 92085-01-03-03. In order to show the change in the part A and part B spectra, the part B spectrum is fitted using part A model parameter values. A clear excess is observed in part B in the 6–15 keV energy range.

(A color version of this figure is available in the online journal.)

is true), especially in order to understand the properties of the new disk (which formed from the condensation of hot matter) and the indigenous disk (standard Keplerian disk).

The observed lag timescales suggest that the geometry of the accretion disk changes, which is strongly supported from spectral studies. The lag was found when the source was in the IM state. Our temporal and spectral variation during the anti-correlated soft lag indicates a truncated accretion disk geometry in the IM state. Similar kinds of studies can be extended to neutron star systems and cataclysmic variables to constrain the geometry of the accretion disk in a specific phase of accretion.

We thank the anonymous referee for constructive and critical comments. We acknowledge the use of *RXTE* data from the HEASARC public archive. This work is also based on observations made with *INTEGRAL*, an ESA science mission with instruments and science data center funded by ESA member states and with the participation of Russia and the USA. This research has made use of data obtained through HEASARC Online Service, provided by NASA/GSFC, in support of the NASA High Energy Astrophysics Programs.

REFERENCES

Arnaud, K. A. 1996, in ASP Conf. Ser. 105, Astronomical Data Analysis Software and Systems V, ed. G. H. Jacoby & J. Barnes (San Francisco, CA: ASP), 17
Belloni, T. 2010, Lecture Notes in Physics, Vol. 794, The Jet Paradigm (Berlin: Springer)
Belloni, T., Mendez, M., van der Klis, M., Hasinger, G., Lewin, W. H. G., & van Paradijs, J. 1996, ApJ, 472, L107
Bevington, P. R., & Robinson, D. K. 1992, Data Reduction and Error Analysis for the Physical Sciences (2nd ed.; New York: McGraw-Hill)
Caballero-García, M. D., Miller, J. M., Trigo, M. D., Kuulkers, E., Fabian, A. C., Mas-Hesse, J. M., Steeghs, D., & van der Klis, M. 2009, ApJ, 692, 1339
Cabanac, C., Henri, G., Petrucci, P. O., Malzac, J., Ferreira, J., & Belloni, T. M. 2010, MNRAS, 404, 738
Casella, P., Belloni, T., Homan, J., & Stella, L. 2004, A&A, 426, 587
Casella, P., Belloni, T., & Stella, L. 2005, ApJ, 629, 403
Chakrabarti, S. K., & Manickam, S. G. 2000, ApJ, 531, L41
Choudhury, M., & Rao, A. R. 2004, ApJ, 616, L143
Choudhury, M., Rao, A. R., Dasgupta, S., Pendharkar, J., Sriram, K., & Agrawal, V. K. 2005, ApJ, 631, 1072
Corbel, S., Fender, R. P., Tzioumis, A. K., Nowak, M., McIntyre, V., Durouchoux, P., & Sood, R. 2000, A&A, 359, 251
Cui, W. 1999, ApJ, 524, L59
Cui, W., Zhang, S. N., & Chen, W. 2000, ApJ, 531, L45
Del Santo, M., et al. 2009, MNRAS, 392, 992
Dickey, J. M., & Lockman, F. J. 1990, ARA&A, 28, 215
Done, C., Gierlinski, M., & Kubota, A. 2007, A&AR, 15, 1
Done, C., & Kubota, A. 2006, MNRAS, 371, 1216
Dunn, R. J. H., Fender, R. P., Körding, E. G., Belloni, T., & Cabanac, C. 2010, MNRAS, 403, 61
Esin, A. A., McClintock, J. E., & Narayan, R. 1997, ApJ, 489, 865
Fender, R. P., Belloni, T., & Gallo, E. 2004, MNRAS, 355, 1105
Fender, R. P., Homan, J., & Belloni, T. M. 2009, MNRAS, 396, 1370
Gallo, E., Corbel, S., Fender, R. P., Maccarone, T. J., & Tzioumis, A. K. 2004, MNRAS, 347, L52
Gallo, E., Fender, R. P., & Pooley, G. G. 2003, MNRAS, 344, 60
Grove, J. E., Johnson, W. N., Kroeger, R. A., McNaron-Brown, K., Skibo, J. G., & Phlips, B. F. 1998, ApJ, 500, 899
Hynes, R. I., Steeghs, D., Casares, J., Charles, P. A., & O'Brien, K. 2003, ApJ, 583, L95
Hynes, R. I., Steeghs, D., Casares, J., Charles, P. A., & O'Brien, K. 2004, ApJ, 609, 317
Jahoda, K., Markwardt, C. B., Radeva, Y., Rots, A. H., Stark, M. J., Swank, J. H., Strohmayer, T. E., & Zhang, W. 2006, ApJS, 163, 401
Kubota, A., Maksishima, K., & Ebisawa, K. 2001, ApJ, 560, L147
Lebrun, F., et al. 2003, A&A, 411, L141
Lei, Y. J., Qu, J. L., Song, L. M., Zhang, C. M., Zhang, S., Zhang, F., Wang, J. M., Li, Z. B., & Zhang, G. B. 2008, ApJ, 677, L461
Levine, A. M., Bradt, H., Cui, W., Jernigan, J. G., Morgan, E. H., Remillard, R., Shirey, R. E., & Smith, D. A. 1996, ApJ, 469, L33
Lin, D., Smith, I. A., Liang, E. P., & Bottcher, M. B. 2000, ApJ, 543, L141
Liu, B. F., Taam, R. E., Meyer-Hofmeister, E., & Meyer, F. 2007, ApJ, 671, 695
Lund, N., et al. 2003, A&A, 411, L231
Mas-Hesse, J. M., et al. 2003, A&A, 411, L261
McClintock, J. E., & Remillard, R. A. 2004, in Compact Stellar X-ray Sources, ed. W. H. G. Lewin & M. van der Klis (Cambridge: Cambridge Univ. Press), 157 (arXiv:astro-ph/0306213)
McClintock, J. E., Remillard, R. A., Rupen, M. P., Torres, M. A. P., Steeghs, D., Levine, A. M., & Orosz, J. A. 2009, ApJ, 698, 1398
Mendez, M., & van der Klis, M. 1997, ApJ, 479, 926
Meyer, F., Liu, B. F., & Meyer-Hofmeister, E. 2007, A&A, 463, 1
Meyer-Hofmeister, E. 2004, A&A, 423, 321
Miller, J. M. 2007, ARA&A, 45, 441
Miyamoto, S., Kimura, K., Kitamoto, S., Dotani, T., & Ebisawa, K. 1991, ApJ, 383, 784

Miyamoto, S., & Kitamoto, S. 1991, ApJ, 374, 741
Motta, S., Belloni, T., & Homan, J. 2009, MNRAS, 400, 1603
Qu, J. L., Lu, F. J., Lu, Y., Song, L. M., Zhang, S., Ding, G. Q., & Wang, J. M. 2010, ApJ, 710, 836
Reig, P., Belloni, T., van der Klis, M., Méndez, M., Kylafis, N. D., & Ford, E. C. 2000, ApJ, 541, 883
Reis, R. C., Miller, J. M., & Fabian, A. C. 2009, MNRAS, 395, L52
Remillard, R. A., & McClintock, J. E. 2006, ARA&A, 44, 49
Rothschild, R. E., Matteson, J. L., Heindl, W., Peterson, L. E., & Hink, P. L. 1995, Proc. SPIE, 2518, 13
Sriram, K., Agrawal, V. K., Pendharkar, J. K., & Rao, A. R. 2007, ApJ, 661, 1055
Sriram, K., Agrawal, V. K., & Rao, A. R. 2009, Res. Astron. Astrophys., 9, 901
Swank, J. 1999, Nucl. Phys. B, 69, 12
Timmer, J., & Koenig, M. 1995, A&A, 300, 707
Titarchuk, L., & Fiorito, R. 2004, ApJ, 612, 988
Ubertini, P., et al. 2003, A&A, 411, L131
Vedrenne, G., Roques, J. P., & Schonfelder, V. 2003, A&A, 411, L63
Winkler, C., et al. 2003, A&A, 411, L1
Wu, K., Soria, R., Hunstead, R. W., & Johnston, H. M. 2001, MNRAS, 320, 177
Zdziarski, A. A., Gierlinski, M., & Mikolajewska, J. 2004, MNRAS, 351, 791